APPLIED SCIENCES AND ENGINEERING

Powerful UAV manipulation via bioinspired self-adaptive soft self-contained gripper

Xinyu Guo[1,2], Wei Tang[1,2,3]*, Kecheng Qin[1,2], Yiding Zhong[1,2], Huxiu Xu[1,2], Yang Qu[1,2], Zhaoyang Li[1,2], Qincheng Sheng[1,2], Yidan Gao[1,2], Huayong Yang[1,2], Jun Zou[1,2]*

Existing grippers for unmanned aerial vehicle (UAV) manipulation have persistent challenges, highlighting a need for grippers that are soft, self-adaptive, self-contained, easy to control, and lightweight. Inspired by tendril plants, we propose a class of soft grippers that are voltage driven and based on winding deformation for self-adaptive grasping. We design two types of U-shaped soft eccentric circular tube actuators (UCTAs) and propose using the liquid-gas phase-transition mechanism to actuate UCTAs. Two types of UCTAs are separately cross-arranged to construct two types of soft grippers, forming self-contained systems that can be directly driven by voltage. One gripper inspired by tendril climbers can be used for delicate grasping, and the other gripper inspired by hook climbers can be used for strong grasping. These grippers are ideal for deployment in UAVs because of their self-adaptability, ease of control, and light weight, paving the way for UAVs to achieve powerful manipulation with low positioning accuracy, no complex grasping planning, self-adaptability, and multiple environments.

INTRODUCTION

In the fields of unmanned aerial vehicles (UAVs), aerial transportation and manipulation (*1*–*6*) have drawn more attention because they notably extend the capabilities of UAVs (*7*), where UAV grasping plays a crucial role (*8*, *9*). Numerous studies on UAV grasping (*10*–*14*) have been reported to date, including rigid grippers designed to mimic avian claws (*15*–*20*), achieving grasping by establishing precise dynamic models of the entire system (*19*, *21*) or installing a series of sensors on the gripper (*20*). However, these approaches require complex controllers and heavy rigid grippers. Some designs use clever mechanical structures to ensure reliable object grasping while reducing the weight of the overall systems. Nevertheless, they are limited in terms of the shapes and sizes of objects they can grasp and also lessen the likelihood that the UAV will successfully grasp an object (*22*, *23*). In brief, rigid grippers depend on accurate models, sensors' feedback, and high-precision control of UAVs, making UAV grasping challenging. Even worse, most rigid grippers are heavy, have a single grasping mode, are limited in the shape and size of the object to be grasped, and lack self-adaptation.

In recent years, with the rise of soft robotics and soft materials (*24*–*28*), numerous soft grippers have been reported (*29*), with some specifically applied to UAV grasping (*30*–*37*). These grippers are primarily based on pneumatic bending actuators, providing lightweight solutions for UAV grasping. Because of the inherent softness of these grippers, they offer advantages in grasping delicate objects such as glass, live animals, and cardboard. In addition, the softness reduces the complexity of gripper control. However, the shapes of these grippers remain resemble rigid grippers, lacking the ability to achieve shape-adaptive grasping. Potted plants, for example, are difficult to grasp. To enhance adaptability of grasping, a form of entangled grasping has been proposed for designing soft grippers with straight elongated circular tube actuators (*38*–*42*), which provides an interesting grasping form and has strong shape-adaptive ability. However, this type of grasping tends to be random, with less success in grasping regular objects like spheres (*39*). Moreover, these grippers are only capable of grasping lightweight objects and are prone to damage (*38*). These shortcomings prevent their potential applications in UAVs. In addition, bulky setups with 16 pneumatic pumps are required to generate high pressure (>100 kPa) for gripper actuation (*39*) because each actuator in the gripper requires its own air supply, further hindering their potential application in UAVs because of UAVs' limited load capacity.

Smooth tendrils are usually used as inspiration for these soft grippers with entangled grasping forms (*38*–*42*). In nature, tendril plants need external support to grow vertically and to get more sunlight (*43*). Most tendril plants have smooth surfaces (i.e., tendril without surface structures) and, as they grow, can quickly come into contact with nearby stems and branches, relying on winding deformation. They eventually have a strong grasp on these stems and branches. In Darwin's famous paper on the habits of climbing plants, these types of tendrils were described as excellent grapnels, tightly clutching branches like birds perching on them (*44*). The aforementioned entangled grasping forms of grippers (*38*–*42*) draw inspiration from these tendrils. However, these tendrils quite fail to attach themselves to a brick wall because of their smooth surface, which cannot support their weight on the wall. We refer to these tendrils (tendril without surface structures) as tendril climbers. In addition to these smooth tendrils, there is another kind of climbing plant with hook-like structures on its surface (i.e., tendril with surface structures). These tendrils' hooks can interlock with objects for support, enabling them to climb and support their weight (*45*, *46*). Though they also exhibit some winding shapes, the growth of these tendrils is solely dependent on hooks. Consequently, these tendrils can climb up the walls of tall buildings and are excellent climbers (*44*). We refer to this type of tendril (tendril with surface structures) as hook climbers. Tendril climber has stronger adaptability, while hook climber has stronger grasping ability due to their different surfaces.

Inspired by tendril plants, we propose a class of self-adaptive soft self-contained grippers that enable UAV to grasp various objects

[1]State Key Laboratory of Fluid Power and Mechatronic Systems, Zhejiang University, Hangzhou 310027, China. [2]School of Mechanical Engineering, Zhejiang University, Hangzhou 310027, China. [3]Institute of Process Equipment, College of Energy Engineering, Zhejiang University, Hangzhou 310027, China.
*Corresponding author. Email: weitang@zju.edu.cn (W.T.); junzou@zju.edu.cn (J.Z.)

with different sizes and shapes (movie S1) in multiple environments. We design two types of elongated soft eccentric circular tube actuators: one with a smooth surface (i.e., without surface structures), similar to tendril climbers; the other with surface structures, similar to hook climbers. On this basis, we fabricate two types of U-shaped soft eccentric circular tube actuators (UCTAs) by fixing the ends of the elongated soft eccentric circular tube actuators, respectively. We add an appropriate amount of low–boiling point liquid and soft resistance wires into the UCTAs. When voltages are applied to the soft resistance wires, the low–boiling point liquid undergoes a phase transition from liquid to gas. The liquid-gas phase transition mechanism (*47*, *48*) can generate high pressure (>200 kPa), which can make UCTAs to generate winding deformations. Hence, by eliminating the requirement for multiple bulky pumps, the mechanism opens the door to the application of UCTAs in UAV manipulation/grasping. Two types of multiple UCTAs are separately cross-arranged to construct two types of soft grippers, forming self-contained systems that can be directly driven by voltage. Similar to tendrils wrapping around branches, both types of grippers can electrically curl to adapt to the shape of the object, achieving entangled grasping. The gripper without surface structures has a large curve after deformation, allowing for better adaptability to the object's shape, similar to tendril climbers. This makes it ideal for delicate grasping jobs like picking up flowers. Unlike the gripper without surface structures, the curvature of the gripper with surface structures reduces during deformation, resulting in a decrease in adaptability, but an increase in load capacity of the gripper due to that the protruding surface structures can interlock with the object, similar to hook climbers. This kind of gripper is suitable for strong grasping tasks, such as picking up heavy stones. Because of the grippers' self-adaptability, UAV manipulation/grasping can be achieved by the grippers without precise positioning or complex grasping planning, reducing the positioning precision required during UAV object grasping and extending the UAV's capability to grasp objects with various sizes and shapes. The actuators' U-shaped bending allows the UAV to grasp objects directly using simple ways such as hanging or hooking. In addition, the soft grippers can adjust the grasping position by making direct contact with objects. All these features of the soft grippers play a significant role in UAV manipulation due to the fact that UAV itself is difficult to control. Successful UAV grasping of various objects on the ground (movie S1), as well as in challenging scenarios such as tree branches (movie S2) and lakes (movie S3), and UAVs collaborative lifting objects (movie S4) demonstrate that the bioinspired self-adaptive soft self-contained grippers pave the way for UAV to achieve powerful manipulation with low positioning accuracy, no complex grasping planning, self-adaptability, and multiple environments.

RESULTS

Bioinspired design of self-adaptive soft self-contained grippers

In nature, tendril plants can grow vertically by attaching to the surrounding supports. Among these tendril plants, tendril climbers rely on winding deformation for vertical climbing and can generate large bending curvatures to firmly grasp even the slender stems of surrounding plants (Fig. 1A). Different from tendril climbers, hook climbers only rely on their surface hooks for vertical climbing (Fig. 1B), and the bending curvature generated from hook climbers is small. Inspired by these tendril plants, we propose a class of self-adaptive soft self-contained grippers that enable UAV to grasp various objects with different sizes and shapes in multiple environments. Drawing inspiration from tendril climbers, we design a UAV gripper without surface structures. This gripper is actuated by voltage and generates a large bending curvature as it deforms to achieve excellent grasping adaptability, making it more suitable for enveloping delicate objects such as a bouquet of flowers (Fig. 1A). Inspired by hook climbers, we design another UAV gripper with surface structures. Compared to grippers without surface structures, the gripper's adaptability is decreased, but load capacity is increased because the surface structures reduce the deformation curvature but can interlock with the objects after voltage actuation. Therefore, this gripper has a strong grasping and can pick up heavy objects like stones (Fig. 1B).

The entire system consists of a quadcopter platform and a soft gripper (Fig. 1C and fig. S1). Two types of grippers are constructed by arranging two types of multiple UCTAs in a cross pattern, where each UCTA has a varying wall thickness with a hollow interior. The manufacturing process of UCTAs and grippers made in silicone is detailed in Materials and Methods, "Materials and fabrication of our gripper" section and figs. S2 to S5. We fill the UCTAs with an appropriate amount of low–boiling point liquid (Novec 7000) and soft resistance wires, forming a voltage-driven self-contained system, thus eliminating the need for a set of bulky pneumatic pumps. When applying voltage to the resistance wires inside the UCTAs, the low–boiling point liquid in the UCTAs undergoes a phase transition from liquid to gas, which is known as a liquid-gas phase transition driving mechanism (*47*, *48*). This increases the pressure inside the UCTAs and results in a winding deformation similar to tendril plants (Fig. 1D). The surface structures on the UCTA can expand and retract freely, and they protrude as the pressure increases and retract as the pressure decreases (Fig. 1E), which guarantees for the release of objects by disengaging the interlocking between the gripper and the objects. The control circuit of the gripper is shown in Fig. 1C. The flight controller (Pixhawk 2.4.8) sends a signal to change the MOSFET's on-off state, which causes the power to be supplied to the ultra battery elimination circuit (UBEC). The UBEC stabilizes the voltage at 5.2 V and applies it to the resistance wires so as to control the gripper (figs. S6 and S7).

It is challenging to actuate the gripper through a single pneumatic source, because each UCTA has a different pressure range for generating deformation due to inevitable small differences in wall thickness among the UCTAs composing the gripper. Hence, multiple pumps are necessary to independently actuate each UCTA and generate a complete deformation of the gripper, leading to a bulky gripper actuation system (*39*) and hindering its deployment on UAV because of UAV's limited payload capacity. We propose that applying the liquid-gas phase transition driving mechanism to each UCTA creates a self-contained gripper system, where the liquid-gas phase transition is directly controlled by applying voltage to the resistance heating wires, thereby eliminating the need for multiple bulky pumps. The specifications of each resistance wire can be well matched to the deformation of each UCTA, making it suitable for gripper actuation. Compact structure, lightweight, and easy control make the self-contained gripper well suited for UAV manipulation/grasping. In addition, in comparison to straight elongated circular tube actuators (*39*), our U-shaped configuration addresses the randomness of grasping and the difficulty in grasping regular-shaped

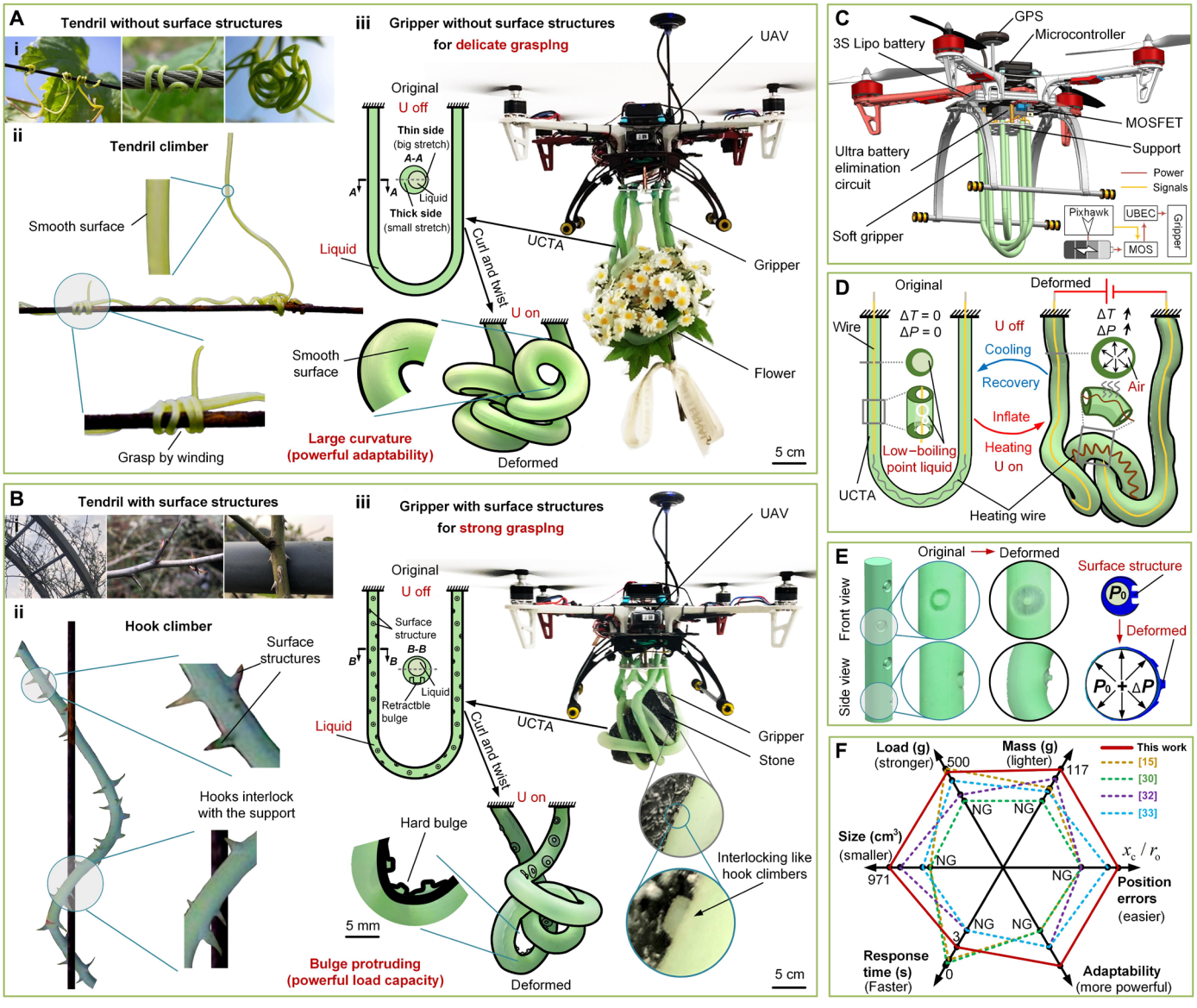

Fig. 1. Bioinspired design of self-adaptive soft self-contained grippers. (**A**) A tendril climber–inspired UAV gripper without surface structures. (i) Photos of tendril climbers. (ii) Tendril climbers rely on winding deformation for climbing and exhibit strong adaptability. (iii) Similar to tendril climbers, the UAV gripper without surface structures we designed relies on winding deformation to grasp objects and exhibits strong adaptability for delicate grasping, such as picking up a bouquet of flowers. (**B**) A hook climber–inspired UAV gripper with surface structures. (i) Photos of hook climbers. (ii) Hook climbers rely on their hooks to climb upwards. (iii) Similar to hook climbers, the UAV gripper with surface structures we designed has hard bulges on the surface that can be embedded in the crevices of the objects and exhibits strong load capacity to grasp heavy objects such as stones. (**C**) Diagram of the mechanical structure and electrical signal transmission for the UAV and gripper. (**D**) Schematic diagram of working principle of the UCTA deformation actuated by liquid-gas phase transitions. (**E**) The principle of retractable surface structures. (**F**) The notable advantages of our gripper compared with other existing grippers deployed on UAVs (*15*, *30*, *32*, *33*) from six aspects. NG means that it is not given.

objects that are placed on the ground (see Materials and Methods, "Comparison with straight elongated circular tube actuators" section). At the same time, the U-shaped gripper extends the grasping modes of the UAV, enabling it to directly grasp objects through simple methods such as hooking and hanging. Compared with existing grippers deployed on UAVs (*15*, *30*, *32*, *33*) (Fig. 1F), our soft self-contained gripper exhibits notable advantages in terms of load, weight, size, response time, adaptability, and positional error (see Materials and Methods, "Methods of quantitative comparison" section and table S1).

Theoretical analysis and simulation of UCTA without surface structures

To quantitatively predict the expansion performance of UCTA during the heating process (voltage on), we conduct theoretical analysis (see Materials and Methods, "Experiments" section). As shown in Fig. 2A, when the temperature of the low–boiling point liquid inside the UCTA increases by ΔT from the initial temperature T_0, the phase transition of the low–boiling point liquid inside the actuator causes a pressure change ΔP (*48*), where P_v (T) is the saturation vapor pressure of the low–boiling point liquid at temperature T

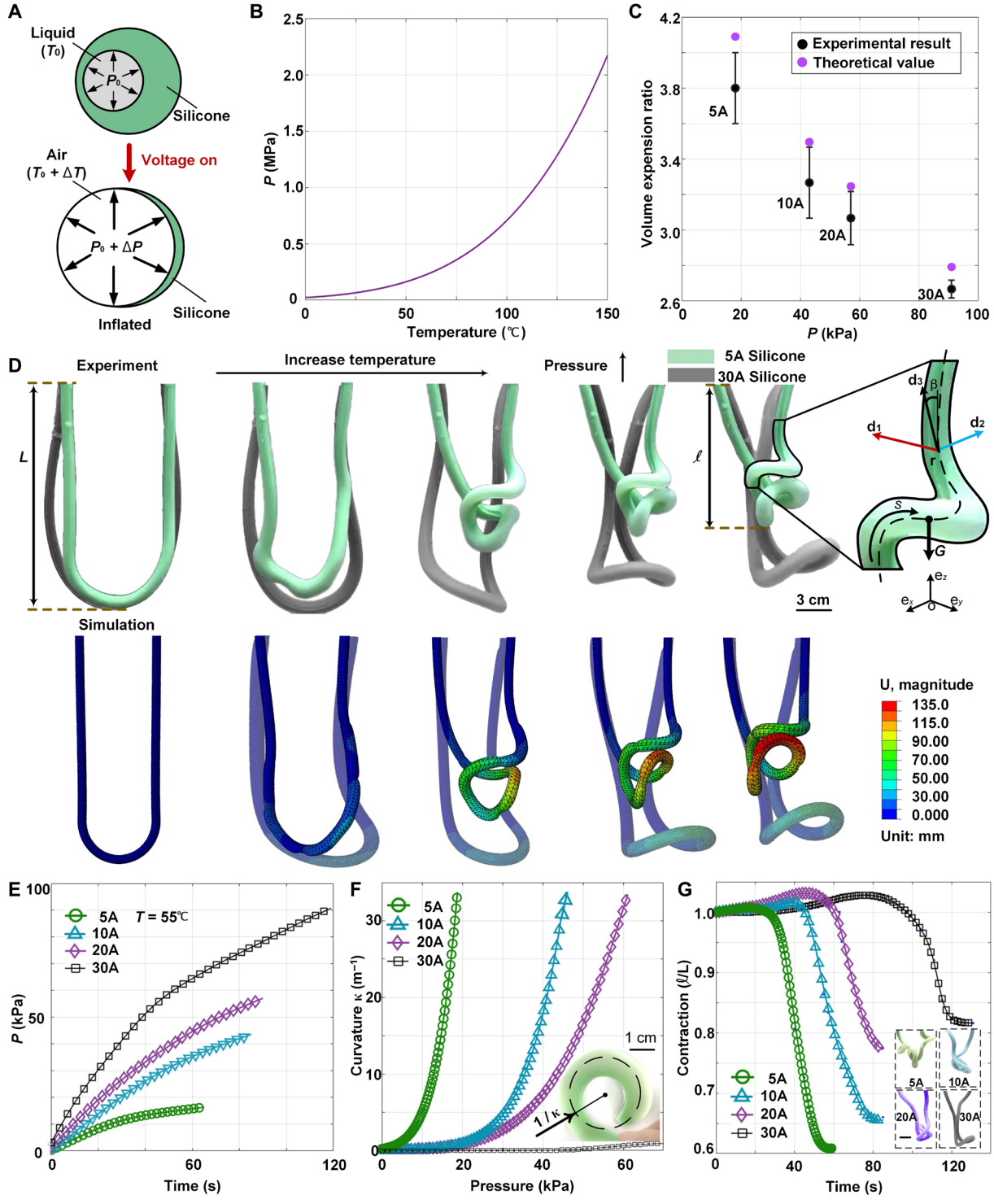

Fig. 2. Theoretical analysis and simulation of UCTA without surface structures. (**A**) The cross section of the UCTA without surface structures during contraction and expansion. (**B**) The saturated vapor pressure property of low–boiling point liquid (Novec 7000). (**C**) By injecting a quantified volume of low–boiling point liquid into the UCTA and heating it, we measure the volume expansion ratio of UCTAs with different hardness materials and the corresponding pressure inside the UCTAs. Error bars indicate the SD of 10 repeated measurements. (**D**) Finite element simulation and experimental results of UCTAs' deformation using materials with hardness of 5A and 30A. The unit tangent $\mathbf{d_3}$ lies along the helix; the unit normal $\mathbf{d_2}$ is horizontal; and the unit binormal $\mathbf{d_1}$ remains perpendicular to $\mathbf{d_3}$ and $\mathbf{d_2}$. The plane containing $\mathbf{d_1}$ and $\mathbf{d_2}$ cuts a cross section through the UCTA. (**E**) Showing the variation in internal pressure of UCTAs made of silicone materials with varying hardness over time at a heating temperature of 55°C. (**F**) The bending curvature κ of UCTAs with different hardness materials under different internal pressures. (**G**) Illustrating the change in contraction over time for UCTA with different hardness materials. Scale bar, 2 cm.

$$\Delta P = P_v(T_0 + \Delta T) - P_v(T_0) \quad (1)$$

The low–boiling point liquid used here is Novec 7000, and its saturation vapor pressure is (*49*)

$$P_v(T) = \exp\left(-\frac{3548.6}{T + 273.15} + 22.978\right) \quad (2)$$

the temperature range for T is $-30°C < T < T_c$, where T_c is the critical temperature of 165°C. The calculated result of the saturated vapor pressure P_v for the selected low–boiling point liquid is shown in Fig. 2B. It is evident that the selected low–boiling point liquid has a maximum saturated vapor pressure of 2.89 MPa. The low–boiling point liquid volume V_l in UCTA affects the deformation and the grasping force of the gripper. Insufficiently loading the UCTA with low–boiling point liquid will not fully deform the gripper, resulting in insufficient grasping force. Excessively loading the UCTA with low–boiling point liquid can cause it to burst. Therefore, the ideal low–boiling point liquid volume V_l should maximize the grasping force without damaging the gripper. To determine the ideal volume V_l of the low–boiling point liquid loaded into the UCTA, we built the volume expansion model (see Materials and Methods, "Volume expansion model" section)

$$\frac{V}{V_0} = RT\frac{V_l\rho}{MP}\frac{4}{\pi d^2 L} + 1 - \varphi \quad (3)$$

where V and V_0 are the expanded volume and initial volume of the UCTA, respectively; ρ and M are the liquid density and molar mass of Novec 7000, respectively; L is the length of the UCTA; R and T are constants; and $\varphi = d^2/D^2$ is the hollow ratio of the UCTA, where d and D are the inner and outer diameters of the UCTA, respectively (*50*). We determined the maximum expansion rate V/V_0 and its corresponding internal pressure P by inflating the UCTA and then calculated the corresponding low–boiling point liquid volume V_l (table S2). On the basis of the volume expansion model, we can quantitatively predict the volume change during the deformation of the UCTA. In addition, it can be observed that the UCTA with a silicone hardness of 5A achieves a volume expansion ratio of up to 400%, indicating sufficient expansion capability to envelop objects. The volume expansion ratio, pressure change, and deformation of the UCTAs made of silicone material with different hardness are shown in Fig. 2 (C to E).

We conduct the following analysis to explain the deformation performance of UCTA and guide the design of UCTA. The eccentric circular tube actuator will bend alone its whole length with a uniform curvature of κ if it is merely subjected to internal air pressure. The relationship between the curvature κ and internal air pressure P is as follows (*38*)

$$\frac{1}{2}\kappa D \sim \left[\frac{P}{G}\left(\frac{D}{2h_f}\right)^{\frac{\alpha-1}{\alpha}}\right]^{\alpha} \quad (4)$$

where G is the shear modulus of silicone rubber, h_f is the thin film thickness of the UCTA, and α is a constant. It can be observed that once the outer diameter D and material of the UCTA are determined, the curvature κ depends on the wall thickness h_f and the internal pressure P. At the same internal pressure P, UCTAs with thin wall thickness h_f can generate significant bending curvature κ (fig. S8A) and curling force F (fig. S8B). However, if the wall thickness wall h_f is too small (<0.6 mm), the deformed surface of the UCTA will develop significant wrinkles that cannot fully recover. We selected $h_f = 0.85$ mm for the gripper construction. The curves in Fig. 2F show the relationship between deformation curvature and internal air pressure for silicone materials with different hardness. Taking gravity into account, the UCTA will extend in the direction of gravity in addition to bending with a uniform curvature κ, forming a three-dimensional helical structure (Fig. 2D). The formed space curve is defined in terms of the position of its centerline $\mathbf{r}$ and an orthonormal director basis $\mathbf{d_1}$, $\mathbf{d_2}$, $\mathbf{d_3}$. The curvature $\boldsymbol{\kappa_{12}}$, which can be decomposed into $\boldsymbol{\kappa_1}$ and $\boldsymbol{\kappa_2}$, lies alone the direction of the unit normal $\mathbf{d_2}$ to the curve and is the rate of change of the unit tangent $\mathbf{d_3}$ as we move along the curve. The twist $\boldsymbol{\kappa_3}$ is a measure of the rate at which the curve is twisting out of the local plane with a binormal $\mathbf{d_1}$ (*51*). We define $\kappa_i = \frac{1}{2}[(\mathbf{e}_i \times \mathbf{e}_j)\cdot\mathbf{e}_k](\mathbf{d}_j' \cdot \mathbf{d}_k)$, with primes denoting derivation with respect to s (*52*). Here, we model the UCTA as a naturally curved rod with an intrinsic curvature that varies upon inflation (*38*). The energy ε of the rod is then written as an integral of the strain energy and gravitational potential energy (*52*)

$$\varepsilon = \int_0^{L_0}\left\{\frac{1}{2}\left[(\kappa_1 - 1)^2 + {\kappa_2}^2 + C{\kappa_3}^2\right] - w_0 s\cos\beta\right\}ds \quad (5)$$

where L_0 is the dimensionless length of the curve; C is the ratio between the twisting and bending moduli; w_0 is the dimensionless weight; and β is the angle between the tangent $\mathbf{d_3}$ and the vertical $\mathbf{e_z}$ (see Materials and Methods, "Naturally curved rod model" section). It can be found that the control parameters of the curved rod are its dimensionless length L_0 and weight w_0. We determined the wall thickness h_f of the UCTA, i.e., the value of the dimensionless mass w_0 was determined. The appropriate length of the UCTA is then selected on the basis of the phase diagram of the rod configuration (*52*), ensuring that the UCTA deforms to a nonplanar global helical configuration, as opposed to a planar or nonplanar localized helical configuration. The deformation processes of UCTAs with different hardness are displayed in fig. S9. Representing the degree of deformation by the stretch ratio ℓ/L, the UCTA with a material hardness of 5A can contract to 60% of its initial length, indicating a large contraction range (Fig. 2G). Furthermore, when the material hardness reaches 30A, the actuating pressure of the UCTA (>100 kPa) exceeds the maximum positive pressure that a miniature rigid pump can provide (~80 kPa), while it can be easily achieved using liquid-vapor phase transitions (>200 kPa).

In conclusion, we find that the UCTA with a silicone hardness of 5A requires the least amount of time to completely deform, resulting in a large curvature (30 m^{-1}), high contraction ratio (40%), and large volume expansion ratio (400%). Therefore, using silicone material with a hardness of 5A is the most suitable for constructing the gripper. However, a 30A silicone gripper is required in scenarios needing very high output force. To guide the design of UCTA, we use an equivalent method to analyze the deformation during pressurization through finite element simulation (see Materials and Methods, "Simulation of deformation" section). In addition, we introduce random perturbations in the finite element analysis to simulate potential defects within the UCTA. The model's accuracy is validated by the anticipated results, which agrees well with experimental data (Fig. 2D).

Principle of UCTA with surface structures

In nature, hook climbers have surface hooks that can interlock with nearby supports, enabling them to overcome their own weight and rise. Inspired by hook climbers, we design UCTA with surface structures (Fig. 3, A and B). When the internal pressure of the UCTA increases, hook-like bulges on its surface made of a harder 30A silicone protrude outward, enhancing the gripper's capacity to grasp heavy objects by embedding into the surface crevices of the objects and creating an interlocking similar to hook-climbers. As the internal pressure decreases, these surface bulges retract to guarantee the object's release. Finite element method is applied to analyze the displacement and cross-sectional stress of UCTA with surface structures (Fig. 3A).

We demonstrated the effectiveness of the surface structures in enhancing the load capacity of UCTA through a set of control experiments, as shown in Fig. 3 (C to E). Two types of UCTAs wrapped around a transparent plastic cup with grooves on the surface, and weights were continuously added to the cup until the entire system becomes unstable. Through 10 repeated experiments, there is a ~29% increase in load capacity for a single UCTA with surface structures

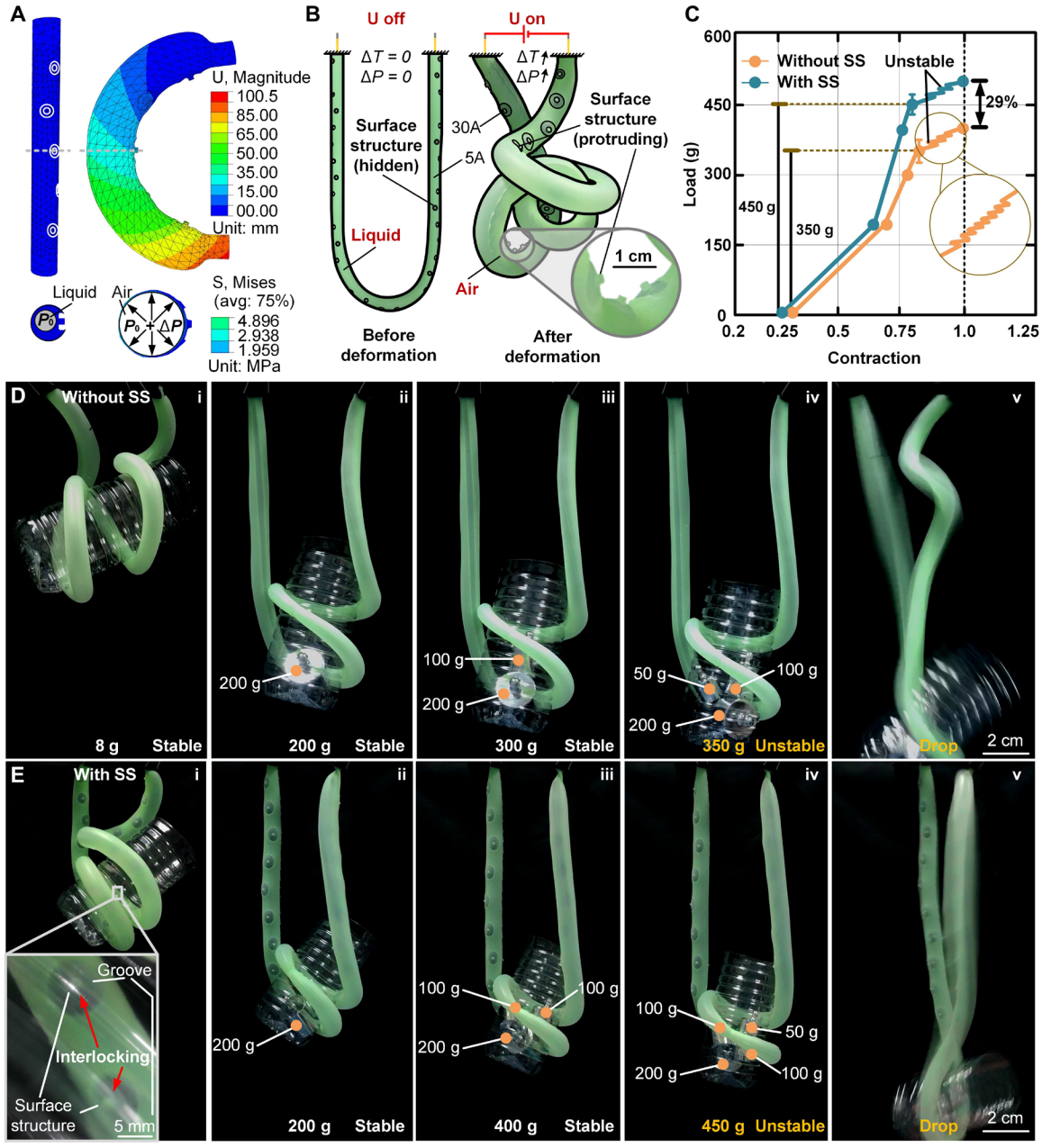

Fig. 3. Principle of UCTA with surface structures. (**A**) Using the finite element method to analyze the displacement and cross-sectional stress of UCTA with surface structures. (**B**) Before and after voltage-driven deformation of UCTA with surface structures. (**C**) Comparison of load capacity data of UCTA with or without surface structures. "SS" means surface structures. Error bars indicate the SD of 10 repeated measurements. (**D**) Load capacity of UCTA without surface structures. (**E**) Load capacity of UCTA with surface structures. The enlarged image shows the protruding bulges embedded in the groove of the plastic cup.

compared to one without, as it can grasp a maximum weight of ~450 g compared to ~350 g for the UCTA without surface structures (movie S5). The load capacity of the gripper constructed from multiple UCTAs is stronger than a single UCTA. However, the presence of surface structures reduces the curvature when the UCTA deforms, because the thickness difference on the upper and lower sides of the UCTA decreases, leading to a reduction in stretching differences. Consequently, grasping adaptability is decreased in the UCTA with surface structures (see Materials and Methods, "Surface structure" section and fig. S10). Nevertheless, the adaptability of grippers constructed from multiple UCTAs with or without surface structures still remains powerful. Gripper without surface structures is excellent for delicate grasping, and gripper with surface structures is suitable for situations requiring a high load capacity. The grippers' self-adaptive capacity enables UAV grasp objects without precise positioning or complex grasping planning, which is undoubtedly of great significance for UAV manipulation.

Actuation process of soft self-contained gripper

To obtain the temperature changes during entire deformation process of UCTA, we used an infrared camera to record both the voltage-on heating deformation process and voltage-off cooling deformation process of UCTA (Fig. 4, A and B). The fluctuation curve shown in Fig. 4A reflects the degree of UCTA's deformation over time, where the slope of the curve represents the deformation rate of the UCTA. The deformation rate of the UCTA decreased when the low–boiling point liquid was heated to point "a" on the curve by the resistance wires because, as the low–boiling point liquid evaporated and the UCTA expanded, the liquid level of the remaining low–boiling point liquid dropped below the resistance wires, ending the phase transition. When we touched the bottom of the UCTA at point "b," the low–boiling point liquid recontacted the resistance wires and rapidly underwent a phase transition, accelerating the deformation rate and resulting in the complete deformation of the UCTA to stage iii (movie S6). The intervention of UAV would speed up the UCTA's deformation rate because the low–boiling point liquid's phase transition would occur more quickly because of the UAV's shaking and coming into contact with the objects or environment, like the ground (movie S7). This means that the combination of UAV and our soft self-contained gripper is complementary: The UAV's shaking promotes the actuating speed of the soft self-contained gripper, and the soft self-contained gripper enhances the grasping capabilities of the UAV.

The voltage-driven process of UAV aerial grasping takes 38 s to achieve full expansion (Fig. 4C, fig. S11, and movies S7 and S8). In addition, we submerged the liquid-gas phase-transition–driven self-contained gripper for testing, and the results showed that the gripper could accomplish expansion and deformation underwater (Fig. 4D). Furthermore, unlike the "ab region of the curve shown in Fig. 4A, there was no decrease in deformation rate when the gripper deformed underwater, and the time to reach full expansion is slightly reduced (~35 s). The reason for the phenomenon is that the effect of buoyancy is gradually greater than that of gravity as the volume of the UCTA grows, causing the gripper to rise and the low–boiling point liquid inside the UCTA to come into contact with the whole length of the resistance wire, thus speeding up the UCTA's deformation (movie S9). The complete deformation time in both the air and underwater takes more than 30 s, as the resistance wires take some time to make a large amount of low–boiling point liquid phase transition. Thus, in practice, the resistance wires first heat for a period of time to induce a phase transition in part of the low–boiling point liquid, resulting in an internal prepressure that would not tighten the gripper but speeds up the grasping time as short as 3 s (movie S10 and fig. S12). Inevitably, preheat method will introduce some drawbacks. When this method is used, the pressure inside the UCTA increases, the stiffness of the UCTA increases, the adaptability of the gripper weakens, and a partial deformation of the gripper occurs, which would bring some limitations on the shape of the grasping objects.

Powerful UAV grasping

To demonstrate the powerful grasping capability of the proposed UAV gripper, we use the UAV to grasp a variety of shapes and sizes of objects indoors. The grasping process can be divided into three steps: The UAV moves toward the target object, allowing the gripper to make contact with the object and adjust the grasping position; the resistance wire then heats the low–boiling point liquid, causing the gripper to expand and grasp the target object; last, the UAV ascends to complete the grasping task. Our soft gripper can continuously make contact with the object to adjust the grasping position during the whole grasping process, which is challenging for rigid grippers because they may move or damage objects while in touch with them and also disturb the flight of the UAV. In addition, similar to tendrils wrapping to adapt to supports, UCTA exhibits adaptability to winding around the shape of each part of the target object during expansion and grasping. By increasing the contact region with the target object, the winding-grasping form lessens the force at contact region and reduces the possibility of object damage. On the contrary, rigid grippers need to apply enough force at limited contact points because of the rigid grippers' grasping form, increasing the risk of damaging the object. Furthermore, the cross-arrangement of UCTAs expands the gripper's coverage area, effectively reducing the required precision for UAV grasping. We demonstrated the powerful manipulation/grasping capability of the UAV through the successful grasping of various objects (Fig. 5 and movie S1), including a regular sphere (Fig. 5A), a dustpan (Fig. 5B), a bottle (Fig. 5C), a goblet (Fig. 5D), an ornament (Fig. 5E), a branch (Fig. 5F), a clamp (Fig. 5G), and a detergent bottle (Fig. 5H).

Our gripper has the ability to grasp objects in the second mode. UAV can directly grasp objects by easily hooking or hanging because of the actuator's U shape, which is useful for difficult UAV aerial grasping and cannot achieve by the aforementioned straight elongated circular tube actuators (*38*–*42*). In addition, the gripper's load capacity is further increased by the hook and hang modes (Fig. 5, G and H), and the gripper is able to lift an object with a mass of 500 g (Fig. 5H), which is about the maximum load of the UAV used in the experiment.

Applications

To demonstrate the practical capabilities of our gripper, we conduct outdoor UAV manipulation experiments without precise positioning or complex grasping planning. We used a UAV to retrieve a set of keys that were suspended from a tree limb (Fig. 6A), demonstrating the gripper's adaptability and the advantage of dual-mode grasping. The UAV flied toward the keys and was able to take down the keys from the tree limb, firstly by the hanging grasp mode, thanks to the self-adaptive gripper that could pass through the tree limbs. Subsequently, the gripper expanded and deformed to firmly grasp

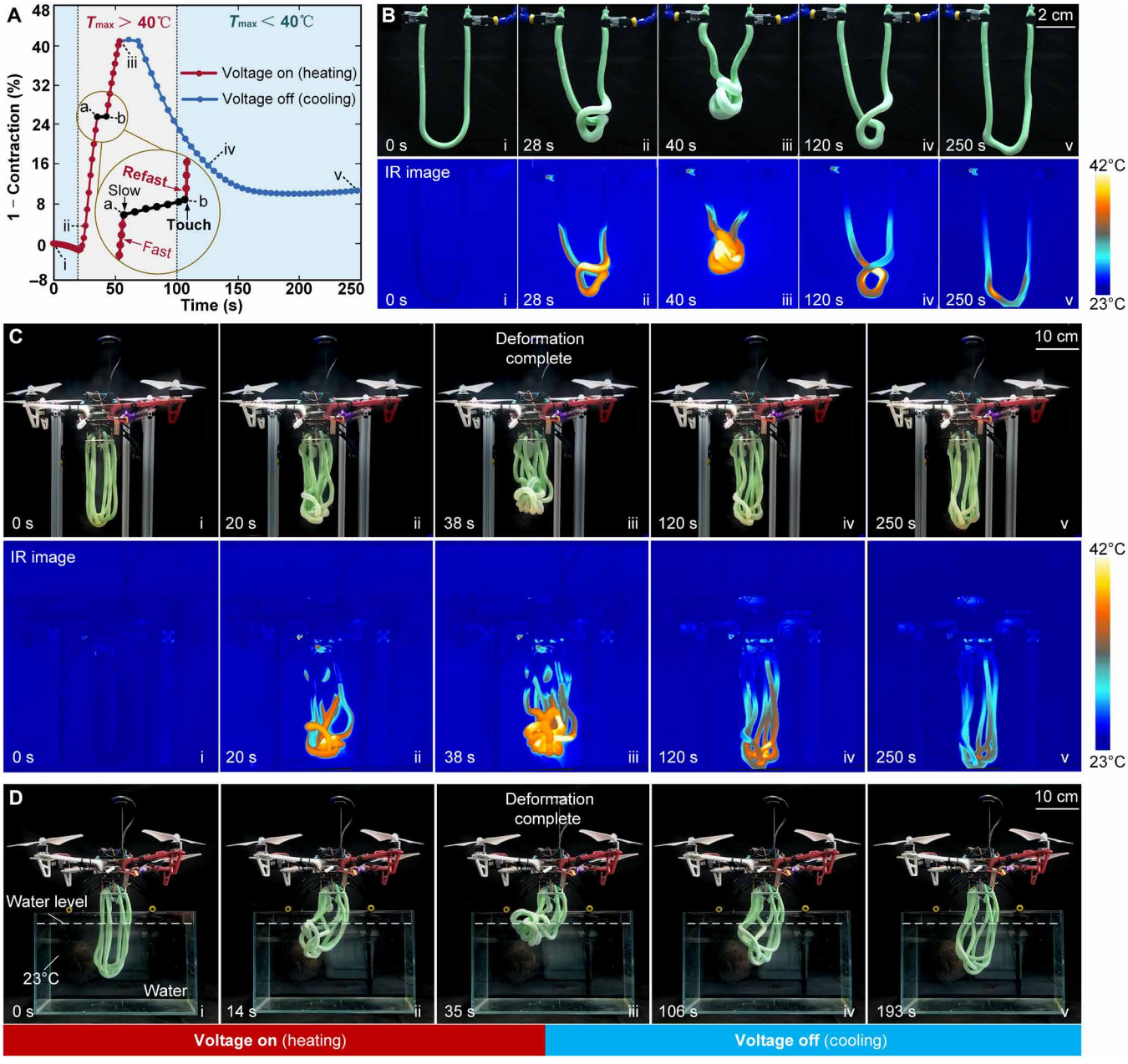

Fig. 4. Actuation process of soft self-contained gripper. (**A**) Deformation-time curve of the UCTA. The gray background color indicates that the maximum temperature inside the gripper is greater than 40°C, and the blue background color indicates that the maximum temperature inside the gripper is lower than 40°C. (**B**) Single UCTA's deformation process and temperature record. IR, infrared. (**C**) Gripper's deformation process and temperature record. (**D**) Deformation process of the gripper underwater.

the keys and completed the grasping task when a voltage was applied to the resistance wires (movie S2). It is challenging for other rigid or soft grippers to pass through the tree limbs and remove such small objects because these grippers may inadvertently grasp fixed tree limbs during the grasping process, resulting in grasp failure.

Garbage cleanup in water is a serious issue that calls for great concern, as it damages the living conditions of marine organisms (*53*). In freshwater ecosystems such as lakes and ponds, manual collection is the main method for garbage cleanup, which is labor intensive (*54*). The UAV's aerial mobility enables rapid movement through water surfaces or across water, providing a strategic advantage in the application of UAV for garbage cleanup in water. We use a UAV to salvage a branch suspended in the lake, demonstrating the feasibility of deploying UAV with the proposed gripper for water garbage cleanup (Fig. 6B). The UAV flied to a specific lake area and immersed the gripper in the lake. Accompanied by the underwater salvage action of the UAV, the U-shaped elongated gripper could hook up the branch. Subsequently, the self-contained system stably provided gas underwater, causing the gripper to expand and tighten its grasp on the object, and the UAV lastly ascended and returned to

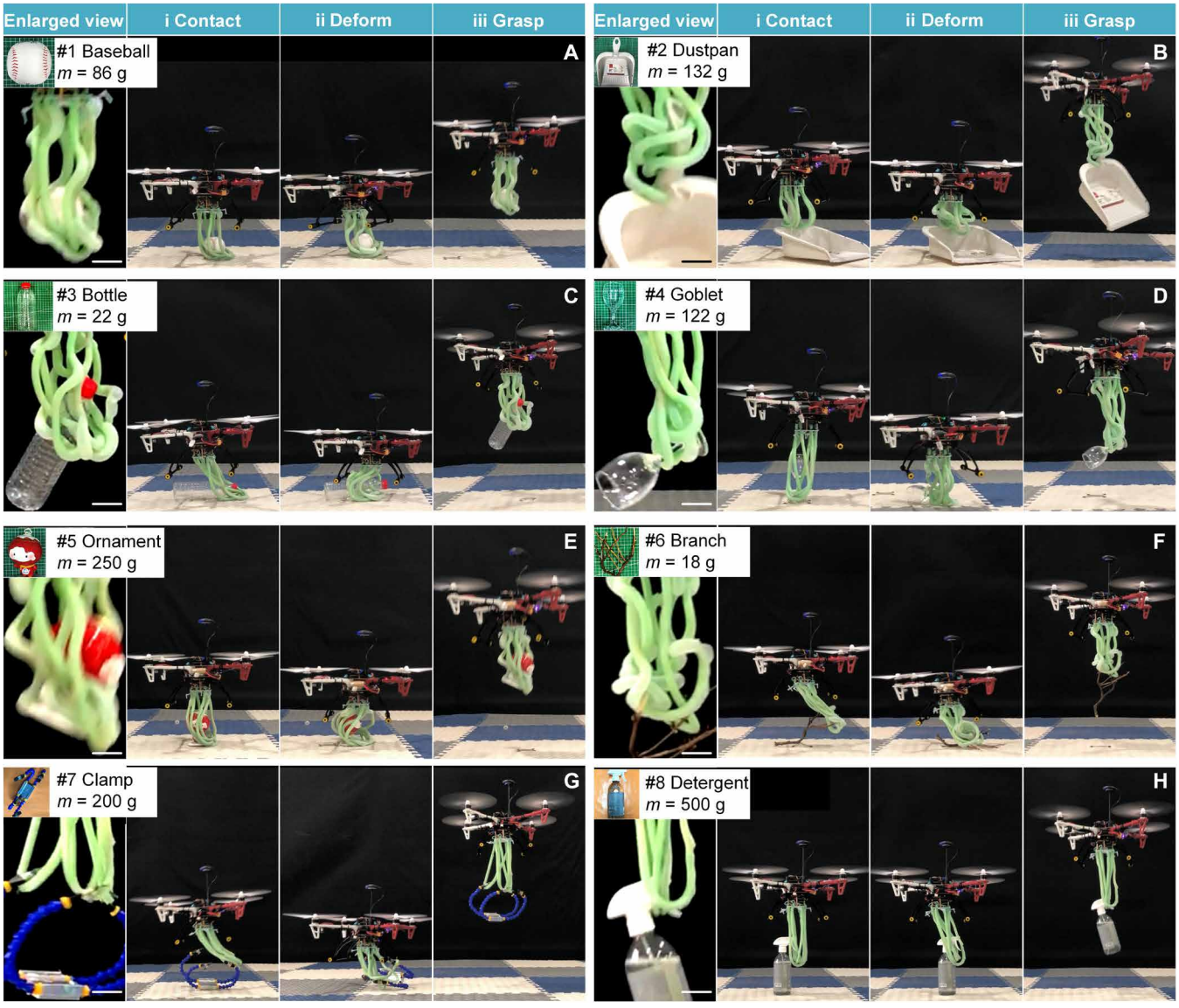

Fig. 5. Experiments of UAV grasping various objects indoors. (**A**) Pictures of the UAV grasping a tennis ball. (**B**) Pictures of the UAV grasping a dustpan. (**C**) Pictures of the UAV grasping a bottle. (**D**) Pictures of the UAV grasping a goblet. (**E**) Pictures of the UAV grasping an ornament. (**F**) Pictures of the UAV grasping a branch. (**G**) Pictures of the UAV grasping a clamp. (**H**) Pictures of the UAV grasping a detergent bottle. The object in the background color of the photo is orange, which means that the gripper can grasp such objects directly by hook and hang without phase transition process. All the scale bars in the pictures, 2 cm.

the shore (movie S3). In this demonstration, it is challenging for UAVs to grasp a tree branch suspended in water because the branch is free moving. Nevertheless, the proposed gripper still has advantages over other grippers because the cross-arranged U-shaped actuators can hook the object to limit its further movement before expanding to hold it. Rigid grippers and soft grippers shaped like rigid grippers have difficulties in grasping objects suspended in water by using simple opening and closing motions, which is further hindered by the visual obstruction of the water and the interference of the propeller airflow. The outdoor grasping applications demonstrate our soft grippers' unique advantages in a range of challenging environments, opening the door for low positioning accuracy, no complex grasping planning, and adaptive, multienvironment grasping by UAVs.

It is so impossible to carry or transport larger and heavier objects using a single UAV that handling them requires the collaboration of multiple UAVs. We conducted an experiment involving two UAVs cooperating to transport objects, showing advantages of our soft gripper in UAVs cooperative transportation (Fig. 6C). Unlike rigid grippers that apply rigid constraints during object grasping, the proposed soft and adaptable gripper not only absorbs vibrations transmitted by UAVs but also permits the object to rotate or move within the gripper. Because of their ability to fly in relation to one another when handling object cooperatively, one UAV can hover without changing its position, while the other UAV can move freely in any direction in space (movie S4), which can reduce the control complexity in UAV cooperative transportation, providing an idea for future multi-UAV cooperative operations.

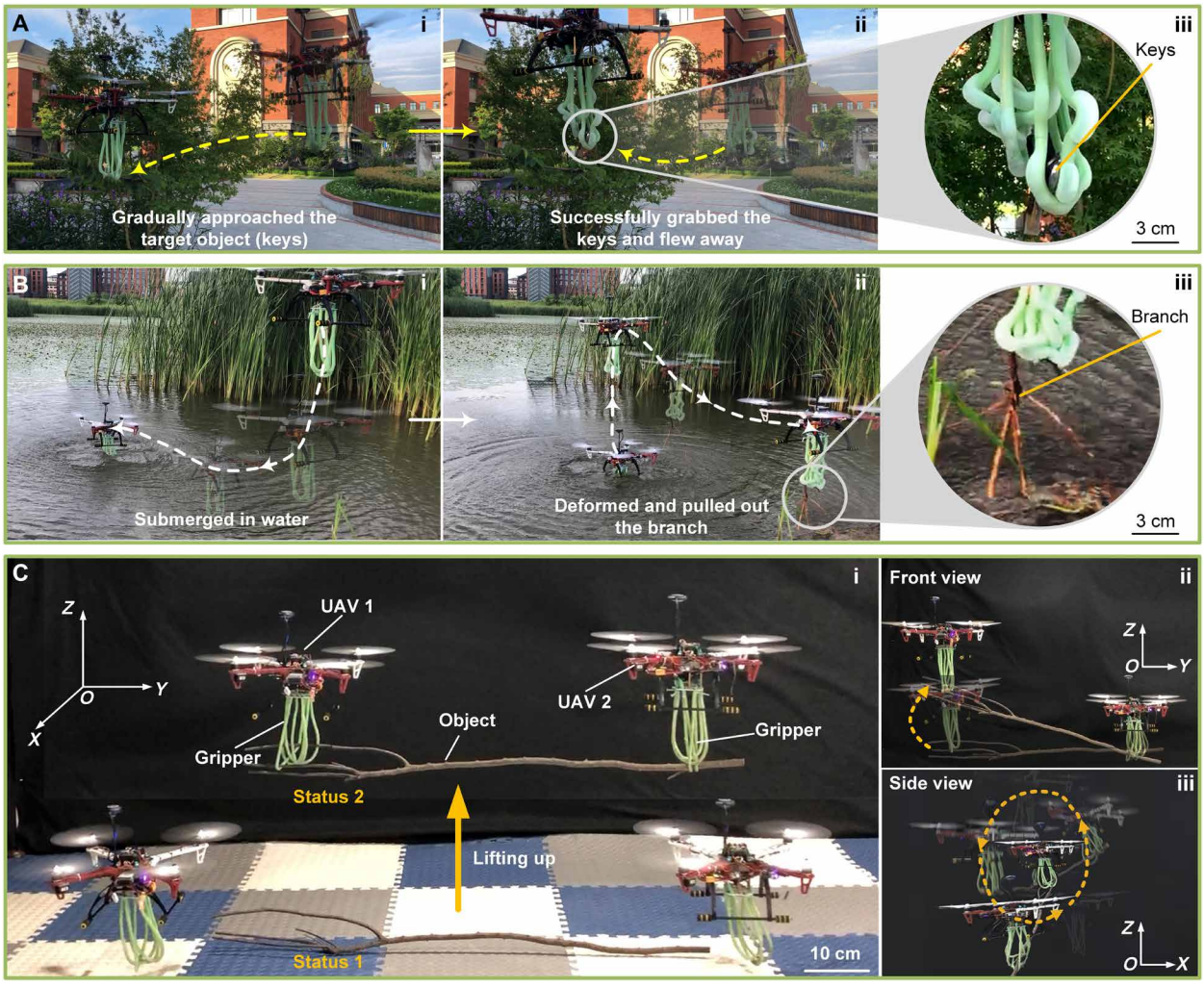

Fig. 6. Practical applications. (**A**) The UAV can take down a set of keys from a tree limb. (**B**) Pictures of the UAV salvaging a branch suspended in the water. (**C**) The scene of two UAVs cooperating to move a large branch. (i and ii) One UAV can move in vertical and horizontal directions relative to another UAV or (iii) rotate around it.

DISCUSSION

In this work, we designed a class of self-adaptive soft self-contained UAV grippers inspired by tendril plants. The grippers are voltage driven and grasp based on winding deformation, allowing UAV to grasp various objects with different sizes and shapes in multiple environments. One of the grippers without surface structures is excellent for delicate grasping, resembling tendril climbers that can generate a large bending curvature. The other gripper with retractable surface structures has high load capacity for strong grasping, similar to hook climbers that can interlock with the objects. These grippers are soft, self-adaptive, self-contained, easy to control, and lightweight, making them ideal for UAV manipulation/grasping. UAV successfully grasps various objects on the ground and in challenging environments such as a lake and a tree limb without precise positioning or complex grasping planning, demonstrating powerful UAV aerial grasping capabilities and paving the way for UAV grasping with low positioning accuracy, no complex grasping planning, self-adaptivity, and multiple environments.

Compared to existing rigid grippers for UAVs (*15*–*20*), our soft self-contained gripper is lightweight and eliminates the need for gripper sensors, accurate models, or high-precision control, offering two grasping modes and safe grasping adaptivity. In comparison to existing soft grippers that are shaped like rigid grippers (*30*–*37*), our soft self-contained gripper has adaptability and dual-mode grasping capabilities to grasp various objects. Unlike soft straight elongated grippers (*38*–*42*), the U-shaped design of our gripper increases the UAV's grasping modes and is more suitable for UAV grasping because it resolves the problems associated with random grasping and unsuccessful grasping of regular objects placed on the ground. In addition, our gripper uses a liquid-gas phase transition mechanism, which eliminates the need for bulky pumps and enables it to be deployed on UAVs that have limited load capacity. Our soft self-contained gripper with the compact, lightweight, and easily controlled structure is outstanding for UAV grasping compared to existing grippers deployed on UAVs (*15*, *30*, *32*, *33*), showcasing superior performance in load, weight, size, response time, adaptability, and position error.

Although our grippers have many valuable properties, there are still some limitations that need to be further improved. The boiling point temperature of the phase transition liquid limits the operating temperature range of the grippers, and the release speed of the gripper is slow. For example, the ambient high temperature will lead to

premature deformation of the grippers, and potential improvements include improving actuator insulation and adding an additional soft container to accelerate gripper release (some attempts can be seen in Materials and Methods "Gripper with an integrated soft container" section, and the release time of the gripper has been notably reduced by ~97%). The grippers' bending curvature and grasping force output can be increased by adding the strain-limiting layers on the thicker side of UCTAs. Independent retractable surface structures are provided to eliminate the influence of surface structures on grippers adaptability, and the distribution density of the surface structures is raised to adapt to the target object with different surface roughness.

Our soft self-contained gripper provides an approach for UAV manipulation. Because the soft and elongated gripper allows friendly human-machine interaction, our gripper can be used for efficient UAVs transportation by winding or hooking objects with manual assistance in challenging transportation terrains, such as steep mountain slopes. In addition, our UAV grasping solution can also be deployed in environmental protection, including gathering trash in the wild and removing garbage from rivers and lakes.

MATERIALS AND METHODS

Materials and fabrication of our gripper

The UCTA was manufactured first. The UCTA without surface structures was cast using molds (fig. S2A) that were 3D printed in polylactic acid (PLA) with a Bambu Lab X1C printer. First, coated all internal molds surfaces with a release agent (Ease Release 200 spray, Mann Release Technologies) to facilitate the removal of the cured silicone in the demolding step. Then mixed components A and B of 5A silicone (PS6600, Shenzhen Yipin Trading, China) in equal proportions, removed air bubbles from the mixture, and poured the mixture into the bottom of the mold. The bracket (stainless steel) was then placed into the mold to form the internal shape of the UCTA. Slowly placed the top part of the mold on top of the bottom one and continued to fill the molds with the mixture. After the silicone had cured, removed the UCTA from the mold. Passed the resistance heating wires (Cr20Ni80, 0.15 mm, Chuangkai Electronics, China) through the chamber of the UCTA and installed the injection pipe at both ends of the U shape. A silicone binder (Sil-Poxy, Smooth-on, USA) was used to seal both ends of the UCTA and the connection with the injection line. Last, injected the low–boiling point liquid (Novec 7000, 3 M, USA) into the UCTA. Therefore, the low–boiling point liquid could be reinjected after consumption.

The UCTA with surface structures was cast using molds (fig. S3) that were also 3D printed in PLA with a Bambu Lab X1C printer. To ensure that the surface structures were fixed on the thicker side of the UCTA, we set up limit structures in the mold for manufacturing UCTA. We made the UCTA by dividing it into two ends, then gluing these two pieces together, so that we could use shorter rods to form the cavity inside the UCTA. The shorter rod had better stiffness and avoided unevenness in actuator wall thickness due to rod bending. When the silicone was poured, a needle tube was first used to inject a higher-hardness (30A) silicone into a small hole in the mold base, and then 5A silicone was poured in, as in the manufacturing process of UCTA without surface structures.

Multiple UCTAs were made, and they were arranged cross-over and fixed on the support to form the UAV gripper, as shown in the fig. S4. The dimensions of the support are shown in fig. S13.

Comparison with straight elongated circular tube actuators

The gripper composed of straight elongated circular tube actuators (*39*) relies on the mutual entanglement between the ends of each actuator to grasp regular-shaped objects such as balls and cylinders. The chance of entanglement between the ends of the straight elongated circular tube actuators is random. In addition, grasping will fail when regular-shaped objects are placed on the ground, because of the ends of the straight elongated circular tube actuators unable to form an entanglement with each other (fig. S14). The gripper composed of U-shaped actuators can be considered that the ends of two straight elongated circular tube actuators are pre-entangled. As a result, our griper addresses the randomness of the grasping process and the difficulty in grasping regular-shaped objects that are placed on the ground.

Methods of quantitative comparison

We compare the size of grippers based on the volume of the space they occupy or enclose. The gripper size of the "Soft drone (*32*) is the volume of its four soft fingers $V_{sd} = 4\pi r_{sd}^2 l_{sd}$, where r_{sd} and l_{sd} are the radius and length of the soft fingers, respectively. The size of the closed-structure compliant gripper (*33*) is the volume of the space it encloses, denoted by the volume of the hemisphere as $V_{cg} = \frac{4}{6}\pi r_{cg}^3$, where r_{cg} is the radius of the gripper. The size of our gripper is also the volume of the space it encloses, denoted as the volume of the cylinder $V_{gripper} = \frac{\pi D_{gripper}^2}{4} h_{gripper}$, where $D_{gripper}$ is the maximum outer diameter of the gripper consisting of UCTA and $h_{gripper}$ is the height of the gripper. There are no detailed data to calculate the size of stereotyped nature-inspired aerial grasper (SNAG) (*15*) and finger-palm synergistic energy dissipation mechanism (FPSED) (*30*), but they do not show a significant size advantage compared to our gripper. The calculation results and parameter values are shown in table S1.

The response time of the gripper refers to the time from the gripper receiving the relevant signal, such as collision or voltage, to the gripper grasping the object. The SNAG (*15*) and FPSED (*30*) have short response times of 50 and 30 ms, respectively, and our gripper can respond in as fast as 3 s.

To analyze the grippers' tolerance to grasp position error, we introduce the center offset rate x_c/r_o, where r_o is the radius of the object to be grasped and the center offset x_c is the distance from the center of the object to the center of the gripper (fig. S15). The larger the center offset rate allowed in the grasping process, the greater the grippers' tolerance to grasping position error. The center offset rate of the rigid gripper SNAG (*15*), the flexible gripper FPSED (*30*), and the Soft drone gripper (*32*) is 0, because their allowable center offset is approximately 0. The center offset rate of the closed-structure compliant gripper (*33*) and our gripper with the same outside diameter $D_{gripper}$ when grasping the same object are x_c/r_o and $(x_c + \Delta x)/r_o$, respectively (fig. S15). Our gripper has a greater tolerance for positional errors because our gripper allows the outside of the object to exceed the outside diameter of the gripper when grasping.

In general, soft grippers have superior shape adaptability compared to grippers based on rigid techniques (*29*). Our gripper is inspired by natural tendril entanglement grasping, making it more adaptable than the previous soft gripper used for UAVs. Experiments on grasping objects of different sizes and shapes have demonstrated our gripper's excellent adaptability. As a result, our grippers

are more adaptable than other rigid (*15*, *30*) or soft grippers (*32*, *33*) used in UAVs.

Experiments

In the theoretical analysis experiments, the pressure change inside the UCTA was measured using a differential pressure meter (AS510, Xima, China). The curvature of the actuators was measured when counteracting gravity by floating the elastomer on a water bath. The resulting curvature was recorded and measured by fitting a circle to the actuator shape. In the deformation process experiments, temperature changes in the UCTA were recorded using a thermal imager (A615, FLIR, America). The UAV used for the grasping experiment was the DJI F450 frame kit (F450, DJI, China). The UBEC (25A, HOBBYWING, China) was used to provide energy to the gripper after depressurizing the supply voltage.

Volume expansion model

The state equation (*50*) was used to calculate the volume expansion ratio V/V_0 of the UCTA shown in Fig. 2C. The quantity of low–boiling point liquid was loaded into the UCTA and heated, causing it to expand under pressure. Assuming the volume of silicone remained constant during the expansion, the UCTA completed its expansion once the low–boiling point liquid was fully evaporated. The volume V of the UCTA was expressed as Eq. 6, where V_0 is the volume of UCTA before expansion, and V_φ is the volume of UCTA's hollow part. V_g is the volume generated by low–boiling point liquid phase transition, expressed by Eq. 9 using the state equation. The volume expansion ratio of the UCTA can be expressed as Eq. 10. Table S2 provides the definitions and values of parameters

$$V = V_0 + V_g - V_\varphi \tag{6}$$

$$V_0 = \frac{\pi D^2}{4} L \tag{7}$$

$$V_\varphi = \frac{\pi d^2}{4} L \tag{8}$$

$$V_g = nRT\frac{1}{P} = RT\frac{V_l\rho}{MP} \tag{9}$$

$$\frac{V}{V_0} = \frac{V_0 + V_g - V_\varphi}{V_0} = RT\frac{V_l\rho}{MP}\frac{4}{\pi d^2 L} + 1 - \frac{d^2}{D^2} \tag{10}$$

Naturally curved rod model

We modeled the UCTA as a naturally curved rod with an intrinsic curvature that varied upon inflation (*38*). The energy ε of the rod was expressed as an integral of the strain energy and gravitational potential energy (*52*)

$$\varepsilon = \int_0^{L_0} \left\{ \frac{1}{2}\left[(\kappa_1 - 1)^2 + {\kappa_2}^2 + C{\kappa_3}^2 \right] - w_0 s\cos\beta \right\} ds \tag{11}$$

The dimensionless weight w_0 could be expressed as $w_0 = w/EI\kappa^3$, where E is the Young's modulus of the elastomer and $w = \frac{1}{4}\rho\pi(D^2 - d^2)g$ means the weight per unit length. The dimensionless length $L_0 = L\kappa$. The ratio between the twisting and bending modulus $C = (1+\nu)^{-1} = \frac{2}{3}$.

Simulation of deformation

Finite element simulations using ABAQUS were conducted to predict the deformation of the UCTA, guiding its design. In ABAQUS, the pressure resulting from the liquid-gas phase transformation of the low–boiling point liquid was applied as a load to the inner surfaces of the UCTA's chamber. The uniaxial tensile tests were performed using an Instron (345 C-05) universal test machine at a speed of 100 mm/min to determine the material properties of the 5A silicone. The specimen's geometry and dimensions were prepared according to method A of the ASTM D412 standard. Each sample underwent visual inspection using a light source directly on the sample to detect and eliminate any bubbles that might remain in the material (*55*). The uniaxial tensile curve of the silicone with different material hardness is shown in fig. S5. We used the test data to fit the hyperelastic material model in Abaqus. The hyperelastic incompressible Yeoh material model (*56*), in which the strain energy $W = C_{10}(I_1 - 3) + C_{20}(I_1 - 3)^2 + C_{30}(I_1 - 3)^3$, was applied to describe the nonlinear material behavior of 5A silicone. The obtained material coefficients were $C_{10} = 0.05$ MPa, $C_{20} = 0.00055$ MPa, and $C_{30} = 0.00021$ MPa. Finite element simulation results for UCTA with material hardness of 5A and 30A are shown in Fig. 2D.

Surface structures

The molds for manufacturing UCTA with surface structures are shown in fig. S3. During manufacturing, a mixture of 30A silicone was first injected into the small holes at the bottom of the mold using a syringe, followed by filling the molds with a mixture of 5A silicone. The geometric dimensions of the surface structures are shown in fig. S16. The surface structures are designed at the maximum wall thickness h_r of UCTA, and the base thickness h_b of the surface structures is less than the wall thickness h_r, resulting in the surface structures protruding when the internal pressure of UCTA rises. The properties of the surface structures are sensitive to the variation of the base thickness h_b. If the base thickness h_b is less than the wall thickness h_f, the surface structures are easy to be damaged before UCTA is completely deformed, because the pressure required for the UCTA to fully deform is larger than the pressure of the protruding surface structures. If the base thickness h_b is greater than the wall thickness h_f, then the surface structures will not protrude during UCTA deformation, because the pressure necessary for the surface structures to protrude is higher than the pressure during UCTA deformation. Therefore, the base thickness h_b is intended to be equal to the wall thickness h_f, and the pressure required for the surface structure to protrude is the same as that required for UCTA deformation, as shown by the white dashed line in fig. S16B. In summary, in the initial state, the surface structures are hidden in the UCTA and can protrude with the deformation of the UCTA when the internal pressure rises, but the surface structures are hidden again when the pressure recovers.

We explored the design parameters of surface structures. The effects of surface structures density on gripper performance are shown in fig. S10. Dense surface structures can reduce UCTA's ability to

deform by twisting; thus, we chose a density of five surface structures per 50 mm to maximize the load capacity of UCTA. Figure S17A illustrates how the bulge base diameter D_{ss} and the bulge diameter d_{ss} affect the grasping force. A large base diameter D_{ss} equipped with a small bulge diameter d_{ss} will result in a low load capacity, as the bulges cannot be firmly embedded in the gaps of the target object. A small base diameter D_{ss} combined with a large bulge diameter d_{ss} will cause the bulges to not fully protrude, reducing the UCTA's load capacity. The influence of distribution form of surface structures on grasping force of gripper is shown in fig. S17B. When the base diameter D_{ss} is 4 mm, the bulge diameter d_{ss} is 2 mm, and the distribution form is (ii), the maximum load of UCTA is ~450 g.

Gripper with an integrated soft container

Additional soft containers (PE, Yuan Dongli, China) are integrated into the gripper design to enhance release speed (fig. S18). During the liquid heating phase, the gripper and the container would remain disconnected. Upon initiation of the release phase, the connection between the gripper and this container would be established, allowing gas to flow into the container. This modification could facilitate a more rapid return of the gripper to its original, undeformed state, reducing the release time of the gripper by ~97%, from ~200 to ~6 s.

Supplementary Materials

This PDF file includes:

Figs. S1 to S18
Tables S1 and S2
Legends for movies S1 to S10

Other Supplementary Material for this manuscript includes the following:

Movies S1 to S10

REFERENCES AND NOTES

1. K. Zhang, P. Chermprayong, F. Xiao, D. Tzoumanikas, B. Dams, S. Kay, B. Bahadir Kocer, A. Burns, L. Orr, C. Choi, D. Dattatray Darekar, W. Li, S. Hirschmann, S. Soana, S. Awang Ngah, S. Sareh, A. Choubey, L. Margheri, V. M. Pawar, R. J. Ball, C. Williams, P. Shepherd, S. Leutenegger, R. Stuart-Smith, M. Kovac, Aerial additive manufacturing with multiple autonomous robots. *Nature* **609**, 709–717 (2022).
2. M. A. Estrada, S. Mintchev, D. L. Christensen, M. R. Cutkosky, D. Floreano, Forceful manipulation with micro air vehicles. *Sci. Robot.* **3**, eaau6903 (2018).
3. H. Liu, H. Tian, D. Wang, T. Yuan, J. Zhang, G. Liu, X. Li, X. Chen, C. Wang, S. Cai, J. Shao, Electrically active smart adhesive for a perching-and-takeoff robot. *Sci. Adv.* **9**, eadj3133 (2023).
4. B. Stephens, L. Orr, B. B. Kocer, H.-N. Nguyen, M. Kovac, An aerial parallel manipulator with shared compliance. *IEEE Robot. Autom. Lett.* **7**, 11902–11909 (2022).
5. L. Li, S. Wang, Y. Zhang, S. Song, C. Wang, S. Tan, W. Zhao, G. Wang, W. Sun, F. Yang, J. Liu, B. Chen, H. Xu, P. Nguyen, M. Kovac, L. Wen, Aerial-aquatic robots capable of crossing the air-water boundary and hitchhiking on surfaces. *Sci. Robot.* **7**, eabm6695 (2022).
6. K. Qin, W. Tang, Y. Zhong, Y. Liu, H. Xu, P. Zhu, D. Yan, H. Yang, J. Zou, An aerial–aquatic robot with tunable tilting motors capable of multimode motion. *Adv. Intell. Syst.* **5**, 2300193 (2023).
7. E. Aucon, S. Kirchgeorg, A. Valentini, L. Pellissier, K. Deiner, S. Mintchev, Drone-assisted collection of environmental DNA from tree branches for biodiversity monitoring. *Sci. Robot.* **8**, eadd5762 (2023).
8. J. Saunders, S. Saeedi, W. Li, Autonomous aerial robotics for package delivery: A technical review. *J. Field Robot.* **41**, 3–49 (2023).
9. H. B. Khamseh, F. Janabi-Sharifi, A. Abdessameud, Aerial manipulation—A literature survey. *Robot. Auton. Syst.* **107**, 221–235 (2018).
10. S.-J. Kim, D.-Y. Lee, G.-P. Jung, K.-J. Cho, An origami-inspired, self-locking robotic arm that can be folded flat. *Sci. Robot.* **3**, eaar2915 (2018).
11. N. Zhao, Y. Luo, H. Deng, Y. Shen, H. Xu, The deformable quad-rotor enabled and wasp-pedal-carrying inspired aerial gripper, in *2018 IEEE/RSJ International Conference on Intelligent Robots and Systems*, Madrid, Spain, 1 to 5 October 2018, pp. 1–9.
12. K. M. Popek, M. S. Johannes, K. C. Wolfe, R. A. Hegeman, J. M. Hatch, J. L. Moore, K. D. Katyal, B. Y. Yeh, R. J. Bamberger, Autonomous grasping robotic aerial system for perching (AGRASP), in *2018 IEEE/RSJ International Conference on Intelligent Robots and Systems*, Madrid, Spain, 1 to 5 October 2018, pp. 1–9.
13. L. Kruse, J. Bradley, A hybrid, actively compliant manipulator/gripper for aerial manipulation with a multicopter, in *2018 IEEE International Symposium on Safety, Security, and Rescue Robotics*, Philadelphia, PA, USA, 6 to 8 August 2018, pp. 1–8.
14. H. Zhang, J. Sun, J. Zhao, Compliant bistable gripper for aerial perching and grasping, in *2019 IEEE International Conference on Robotics and Automation*, Montreal, QC, Canada, 20 to 24 May 2019, pp. 1248–1253.
15. W. R. T. Roderic, M. R. Cutkosky, D. Lentink, Bird-inspired dynamic grasping and perching in arboreal environments. *Sci. Robot.* **6**, eabj7562 (2021).
16. W. Stewart, E. Ajanic, M. Müller, D. Floreano, How to swoop and grasp like a bird with a passive claw for a high-speed grasping. *IEEE-ASME Trans. Mechatron.* **27**, 3527–3535 (2022).
17. W. Stewart, L. Guarino, Y. Piskarev, D. Floreano, Passive perching with energy storage for winged aerial robots. *Adv. Intell. Syst.* **5**, 2100150 (2023).
18. L. Bai, H. Wang, X. Chen, J. Zheng, L. Xin, Y. Deng, Y. Sun, Design and experiment of a deformable bird-inspired UAV perching mechanism. *J. Bionic Eng.* **18**, 1304–1316 (2021).
19. J. Thomas, G. Loianno, J. Polin, K. Sreenath, V. Kumar, Toward autonomous avian-inspired grasping for micro aerial vehicles. *Bioinspir. Biomim.* **9**, 025010 (2014).
20. R. Zufferey, J. Tormo-Barbero, D. Feliu-Talegón, S. R. Nekoo, J. A. Acosta, A. Ollero, How ornithopters can perch autonomously on a branch. *Nat. Commun.* **13**, 7713 (2022).
21. X. Shi, Q. Wang, C. Wang, R. Wang, L. Zheng, C. Qian, W. Tang, An AI-based curling game system for winter olympics. *Research* **2022**, 9805054 (2022).
22. U. A. Fiaz, N. Toumi, J. S. Shamma, Passive aerial grasping of ferrous objects. *IFAC PapersOnLine* **50**, 10299–10304 (2017).
23. H. Hsiao, J. Sun, H. Zhang, J. Zhao, A mechanically intelligent and passive gripper for aerial perching and grasping. *IEEE-ASME Trans. Mechatron.* **27**, 5243–5253 (2022).
24. T. J. Wallin, J. Pikul, R. F. Shepherd, 3D printing of soft robotic systems. *Nat. Rev. Mater.* **3**, 84–100 (2018).
25. S. I. Rich, R. J. Wood, C. Majidi, Untethered soft robotics. *Nat. Electron.* **1**, 102–112 (2018).
26. W. Tang, C. Zhang, Y. Zhong, P. Zhu, Y. Hu, Z. Jiao, X. Wei, G. Lu, J. Wang, Y. Liang, Y. Lin, W. Wang, H. Yang, J. Zou, Customizing a self-healing soft pump for robot. *Nat. Commun.* **12**, 2247 (2021).
27. W. Tang, Y. Lin, C. Zhang, Y. Liang, J. Wang, W. Wang, C. Ji, M. Zhou, H. Yang, J. Zou, Self-contained soft electrofluidic actuators. *Sci. Adv.* **7**, eabf8080 (2021).
28. W. Tang, Y. Zhong, H. Xu, K. Qin, X. Guo, Y. Hu, P. Zhu, Y. Qu, D. Yan, Z. Li, Z. Jiao, X. Fan, H. Yang, J. Zou, Self-protection soft fluidic robots with rapid large-area self-healing capabilities. *Nat. Commun.* **14**, 6430 (2023).
29. J. Shintake, V. Cacucciolo, D. Floreano, H. Shea, Soft robotic grippers. *Adv. Mater.* **30**, 1707035 (2018).
30. Y. Zhang, W. Zhang, P. Gao, X. Zhong, W. Pu, Finger-palm synergistic soft gripper for dynamic capture via energy harvesting and dissipation. *Nat. Commun.* **13**, 7700 (2022).
31. A. McLaren, Z. Fitzgerald, G. Gao, M. Liarokapis, A passive closing, tendon driven, adaptive robot hand for ultra-fast, aerial grasping and perching, in *2019 IEEE/RSJ International Conference on Intelligent Robots and Systems*, Macau, China, 3 to 8 November 2019, pp. 5602–5607.
32. J. Fishman, S. Ubellacker, N. Hughes, L. Carlone, Dynamic grasping with a "Soft" drone: From theory to practice, in *2021 IEEE/RSJ International Conference on Intelligent Robots and Systems*, Prague, Czech Republic, 27 September to 1 October 2021, pp. 4214–4221.
33. L. Y. Lee, O. A. Syadiqeen, C. P. Tan, S. G. Nurzaman, Closed-structure compliant gripper with morphologically optimized multi-material fingertips for aerial grasping. *IEEE Robot. Autom. Lett.* **6**, 887–894 (2021).
34. M. Shatadal, Y. Dangli, T. Carly, P. Panagiotis, Z. Wenlong, Design and control of a hexacopter with soft grasper for autonomous object detection and grasping, in *ASME 2018 Dynamic Systems and Control Conference*, Atlanta, Georgia, USA, 30 September to 3 October 2018.
35. P. Zheng, F. Xiao, P. H. Nguyen, A. Farinha, M. Kovac, Metamorphic aerial robot capable of mid-air shape morphing for rapid perching. *Sci. Rep.* **13**, 1297 (2023).
36. F. J. Garcia Rubiales, P. Ramon Soria, B. C. Arrue, A. Ollero, Soft-tentacle gripper for pipe crawling to inspect industrial facilities using UAVs. *Sensors* **21**, 4142 (2021).
37. K. C. V. Broers, S. F. Armanini, Design and testing of a bioinspired lightweight perching mechanism for flapping-wing MAVs using soft grippers. *IEEE Robot. Autom. Lett.* **7**, 7526–7533 (2022).
38. T. J. Jones, E. Jambon-Puillet, J. Marthelo, P.-T. Brun, Bubble casting soft robotics. *Nature* **599**, 229–233 (2021).
39. K. P. Becker, C. Teeple, N. Charles, Y. Jung, D. Baum, J. C. Weaver, L. Mahadevan, R. J. Wood, Active entanglement enables stochastic, topological grasping. *Proc. Natl. Acad. Sci. U.S.A.* **119**, e2209819119 (2022).
40. K. P. Becker, Y. Chen, R. J. Wood, Soft actuator arrays: Mechanically programmable dip molding of high aspect ratio soft actuator arrays. *Adv. Funct. Mater.* **30**, 2070075 (2020).

41. R. V. Martinez, J. L. Branch, C. R. Fish, L. Jin, R. F. Shepherd, R. M. D. Nunes, Z. Suo, G. M. Whitesides, Robotic tentacles with three-dimensional mobility based on flexible elastomers. *Adv. Mater.* **25**, 205–212 (2013).
42. J. Zou, M. Feng, N. Ding, P. Yan, H. Xu, D. Yang, N. X. Fang, G. Gu, X. Zhu, Muscle-fiber array inspired, multiple-mode, pneumatic artificial muscles through planar design and one-step rolling fabrication. *Natl. Sci. Rev.* **8**, nwab048 (2021).
43. E. Gianoli, The behavioural ecology of climbing plants. *Aob Plants* **7**, plv013 (2015).
44. C. Darwin, On the movements and habits of climbing plants. *Bot. J. Linn. Soc.* **9**, 1–118 (1865).
45. K. J. Niklas, Climbing plants: Attachment and the ascent for light. *Curr. Biol.* **21**, R199–R201 (2011).
46. G. Bauer, M.-C. Klein, S. N. Gorb, T. Speck, D. Voigt, F. Gallenmüller, Always on the bright side: The climbing mechanism of Galium aparine. *Proc. Biol. Sci.* **22**, 2233–2239 (2010).
47. Y. Zhong, W. Tang, C. Zhang, Z. Jiao, D. Wu, W. Liu, H. Yang, J. Zou, Programmable thermochromic soft actuators with "two dimensional" bilayer architectures for soft robotics. *Nano Energy* **102**, 107741 (2022).
48. Y. Zhong, W. Tang, H. Xu, K. Qin, D. Yan, X. Fan, Y. Qu, Z. Li, Z. Jiao, H. Yang, J. Zou, Phase-transforming mechanical metamaterials with dynamically controllable shape-locking performance. *Natl. Sci. Rev.* **10**, nwad192 (2023).
49. 3M. Technical Data: 3M Novec 7000 Engineered Fluid. (2023); https://multimedia.3m.com.cn/mws/media/121372O/3m-novec-7000-engineered-fluid-tds.pdf&fn=3M%20Novec%207000%20Engineered%20Fluid%20TDS%20Heat%20Transfer_FINAL_R3.pdf.
50. K. Narumi, H. Sato, K. Nakahara, Y. A. Seong, K. Morinaga, Y. Kakehi, R. Niiyama, Y. Kawahara, Liquid pouch motors: Printable planar actuators driven by liquid-to-gas phase change for shape-changing interfaces. *IEEE Robot. Autom. Lett.* **5**, 3915–3922 (2020).
51. W. K. Silk, N. M. Holbrook, The importance of frictional interactions in maintaining the stability of the twining habit. *Am. J. Bot.* **92**, 1820–1826 (2005).
52. J. T. Miller, A. Lazarus, B. Audoly, P. M. Reis, Shapes of a suspended curly hair. *Phys. Rev. Lett.* **112**, 068103 (2014).
53. Z. Long, Begin ocean garbage cleanup immediately. *Science* **381**, 612–613 (2023).
54. S. N. Hasany, S. S. Zaidi, S. A. Sohail, M. Farhan, An autonomous robotic system for collecting garbage over small water bodies, in *2021 6th IEEE International Conference on Automation, Control and Robotics Engineering*, Dalian, China, 15 to 17 July 2021, pp. 81–86.
55. L. Marechal, P. Balland, L. Lindenroth, F. Petrou, C. Kontovounisios, F. Bello, Toward a common framework and database of materials for soft robotics. *Soft Robot.* **8**, 284–297 (2021).
56. O. H. Yeoh, Some forms of the strain energy function for rubber. *Rubber Chem. Technol.* **66**, 754–771 (1993).

Acknowledgments
Funding: This work was supported by the International Cooperation Program of the Natural Science Foundation of China under grant no.52261135542 (J.Z.), the National Natural Science Foundation of China under grant no. 52305074 (W.T.), the Zhejiang Provincial Natural Science Foundation of China under grant no. LD22E050002 (J.Z.), China National Postdoctoral Program for Innovative Talents under grant no. BX20220267 (W.T.), and the China Postdoctoral Science Foundation under grant no. 2023 M733066 (W.T.). **Author contributions:** W.T. and J.Z. proposed and supervised the project. X.G., W.T., and J.Z. designed the research. X.G., K.Q., Y.Z., H.X., Y.Q., Z.L., Q.S., and Y.G. conducted the experimental work. X.G. developed theoretical analysis and finite element simulation and analyzed the data. X.G. and W.T. wrote the manuscript with input from all authors. W.T., J.Z., and H.Y. revised the manuscript. **Competing interests:** The authors declare that they have no competing interests. **Data and materials availability:** All data needed to evaluate the conclusions in the paper are present in the paper and/or the Supplementary Materials.

Submitted 20 December 2023
Accepted 8 April 2024
Published 8 May 2024
10.1126/sciadv.adn6642